Molecular Therapy
Methods & Clinical Development
Original Article

# Enhancing titers of therapeutic lentiviral vectors using PKC agonists

Charles Moore-Kelly,[1] Rajesh Reddem,[1] Ben M. Alberts,[1] Jordan Wright,[1] Thomas Evans,[1] Anurag Kulkarni,[1] Nicholas G. Clarkson,[1] Daniel C. Farley,[1] Kyriacos A. Mitrophanous,[1] and Rui André Saraiva Raposo[1]

[1]Oxford Biomedica (UK) Ltd., Windrush Court, Transport Way, Oxford OX4 6LT, UK

**Lentiviral vector (LV)-based therapies employ the molecular machinery of HIV-1 to stably integrate therapeutic genes into patient cells for long-term disease correction. However, suboptimal expression of LV components in HEK293T-based production systems can limit titers and hinder clinical product development. Here, we identify protein kinase C (PKC) agonists as robust enhancers of LV production. PKC activation resulted in rapid transcription of LV genomic RNA and accelerated vector particle release in a manner that complemented the use of the histone deacetylase (HDAC) inhibitor, sodium butyrate. Stimulation of HEK293T cells strongly upregulated AP-1 transcription factor subunits independently of nuclear factor κB (NF-κB) pathway activation. Application of PKC agonists in LV production resulted in a ∼3-fold improvement in the titer of a chimeric antigen receptor (CAR)-LV. Furthermore, a ∼9-fold increase in titer was achieved when this induction method was combined with co-expression of an LV RNA-targeted U1 snRNA enhancer. Importantly, LV produced using PKC agonists had comparable particle-to-infectivity ratios and preserved T cell transduction efficiency. These findings suggest that incorporating PKC agonists into commercial LV manufacturing could considerably reduce the cost per patient dose of new LV-based gene therapies.**

## INTRODUCTION

The use of HIV-1-derived lentiviral vectors (LVs) has become an established method for delivering therapeutic genes into patient cells, particularly for the generation of autologous chimeric antigen receptor (CAR) T cells in treating hematological malignancies.[1,2] However, an ongoing challenge in LV manufacturing is achieving the high production yields required to ensure commercial viability of new cell and gene therapies. The manufacture of 3$^{rd}$ generation LVs in mammalian cells is intrinsically complex, partly due to mechanisms that limit productive plasmid expression or interfere with efficient viral vector assembly.[3–8] Product-to-product differences resulting from the expression of transgene proteins can also impact LV titers and/or processing in a manner that is difficult to predict, driving further demand for the development of technologies to improve upstream productivity.[9,10]

Several strategies have been described to overcome the limiting availability of viral components in the production of self-inactivating (SIN) LVs. In clinical manufacturing, the histone deacetylase (HDAC) inhibitor sodium butyrate is widely used to induce LV expression in transient, packaging, and producer systems.[11–14] Mechanistically, HDAC inhibitors positively drive transcriptional activity by increasing acetylation of the ε-amino group of lysine residues in histone tails.[15] The resulting decondensation of chromatin structure facilitates binding of transcription factors to promote gene expression.[16,17] Induction with sodium butyrate in LV production is frequently reported to increase output titers by an order of magnitude, establishing this operation as a key determinant of yield in many processes.[11,12] The expression of LV genes can also be enhanced through co-expression of viral transactivating proteins, such as Tax or Tat, with considerable impact on titer.[7,18] In an alternative strategy, Han and colleagues demonstrated that transcriptional processivity could be enhanced by overexpressing the elongation factors SPT4 and SPT5, resulting in improved viral RNA (vRNA) completeness and particle release.[19] Previously, our group reported that co-expression of a retargeted U1-snRNA designed to bind across the dimerization sequence of stem loop 1 in the packaging signal (Ψ) can enhance both LV production and quality.[20,21] The optimized sequence, referred to as "256U1", has been shown to increase the availability of packageable vRNA and limit promiscuous splicing between the major splice donor and a splice acceptor located within the EF1α promoter common to many therapeutic products.

In our examination of alternative small molecule drugs with potential to stimulate LV expression, we identified PKC agonists as strong inducers of SIN-LV production in our HEK293T-derived cells. PKC agonists mimic the secondary messenger diacylglycerol to initiate downstream signaling cascades from both classical and novel PKC isoforms.[22] This kinase family integrates signaling networks in an isozyme and cell-type-specific manner to drive transcriptional activity from extracellular signal-regulated kinase (ERK), c-Jun N-terminal kinase (JNK), p38, or nuclear factor κB (NF-κB) pathways.[23] PKC agonists have previously been identified as potent latency reversal

Received 4 February 2025; accepted 2 May 2025;
https://doi.org/10.1016/j.omtm.2025.101484.

**Correspondence:** Charles Moore-Kelly, Oxford Biomedica (UK) Ltd., Windrush Court, Transport Way, Oxford OX4 6LT, UK.
**E-mail:** c.moore-kelly@oxb.com

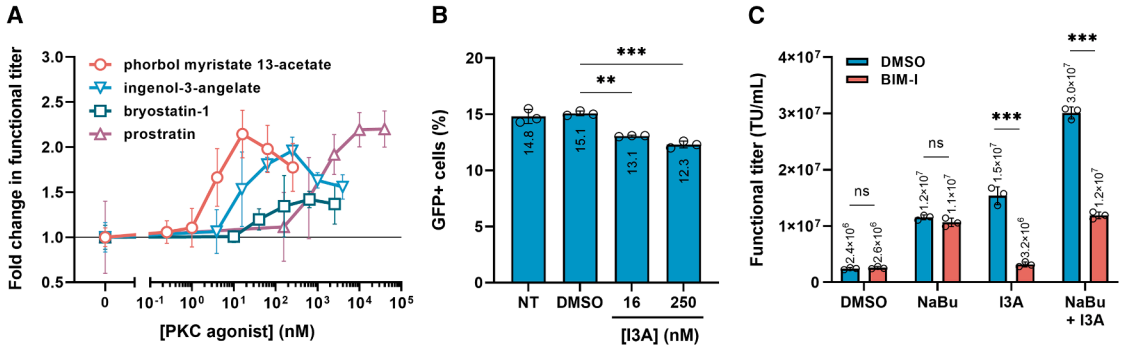


**Figure 1. PKC agonists increase LV titers in HEK293T-derived production cells**

(A) Fold change in functional titer of LV-CMV-GFP produced in suspension-adapted HEK293T using PKC agonists phorbol myristate 13-acetate (red: 250 pM–256 nM), ingenol-3-angelate (blue: 3.9 nM–4 μM), bryostatin-1 (green: 10 nM–2.56 μM), and prostratin (purple: 156 nM–40 μM). PKC agonist or 0.2% (v/v) DMSO was added to media immediately after 10 mM NaBu for all conditions. (B) Impact of residual PKC agonist on reported transduced cells. Percentage of GFP$^+$ HEK293T was determined by flow cytometry three days post-transduction with vector reference control (LV-CMV-GFP) spiked with 16 nM I3A, 250 nM I3A, 0.2% (v/v) DMSO, or untreated (NT). (C) Effect of PKC inhibitor BIM-I on LV-CMV-GFP titer. Transfected cells were pre-treated with 2 μM BIM-I (red) or 0.1% (v/v) DMSO (blue) for 1 h prior to the addition of inducing agents. LV was harvested 24 h after the addition of 0.2% (v/v) DMSO, 10 mM NaBu + 0.2% (v/v) DMSO, 250 nM I3A, or 10 mM NaBu + 250 nM I3A. Functional titers were determined by flow cytometry of HEK293T three days post-transduction. Statistical significance was established using Welch's t test: $^{**}p < 0.01$ and $^{***}p < 0.001$; ns, not significant. All data are mean average values ± SD of biological triplicates ($n = 3$).

agents for their capacity to antagonize HIV-1 dormancy in host T cells.[24,25] This activity is attributed, in part, to the strong activation of NF-κB and its association with the U3 region of the 5′ long terminal repeat of integrated HIV-1 provirus.[26–29] However, the transcription-enhancing activity of PKC agonists has not been characterized in the context of the expression of 3$^{rd}$ generation SIN-LV, where viral components are split across separate cytomegalovirus (CMV) promoter-driven plasmids and the viral genome lacks the 5′ U3 region.[2]

Here we show that PKC agonists can be used to increase the titer of a "model" 3$^{rd}$ generation SIN-LV with GFP reporter transgene via accelerated release kinetics. The benefits of using PKC agonists were further demonstrated in the production of a "low-yielding" therapeutic CAR-LV product,[30] where we observed a strong response to PKC activation that could be further improved by co-expression of the 256U1 snRNA enhancer.[20,21] Analysis of the proteome and phosphoproteome of production cells identified a broad cellular response to PKC activation, which included rapid upregulation of AP-1 transcription factor subunits and post-translational modifications to proteins involved in signaling, transcription, and chromatin modification. In our study, particular focus was given to the use of the FDA-approved PKC agonist ingenol-3-angelate (I3A), which has previously been manufactured to good manufacturing practice (GMP) grade, thereby presenting an opportunity to transition into a clinical LV manufacturing environment.[31]

## RESULTS

### PKC agonists increase LV titers in HEK293T-derived production cells

The PKC agonists phorbol myristate 13-acetate (PMA), I3A, prostratin, and bryostatin-1 were evaluated for their impact on the output titer of a 3$^{rd}$ generation LV containing a GFP reporter transgene (LV-CMV-GFP) (Figure 1A). Suspension-adapted HEK293T production cells were stimulated with PKC agonist immediately after the addition of sodium butyrate (NaBu) 20 h post-transfection. A dose-dependent increase in functional LV titer was observed for all PKC agonists. PMA and prostratin (both phorbol esters), and I3A (a diterpenoid ester) induced a ∼2-fold increase in LV titer with respect to vehicle at optimal concentrations of 16 nM, 10 μM, and 250 nM, respectively. The macrolide lactone bryostatin-1 was found to induce the weakest increase of 1.4-fold at 640 nM. Addition of ≤0.3% (v/v) DMSO immediately after NaBu induction was shown not to have a significant effect on titer with respect to normal LV production procedure (Figure S1).

Next, we showed that residual PKC agonist within LV harvest material was not inflating functional titer values reported by the transduction assay by affecting target cells. A stock of LV-CMV-GFP reference control was spiked with I3A immediately prior to transduction, and the percentage of transduced HEK293T cells was determined at assay termination three days later (Figure 1B). A modest dose-dependent decrease in GFP$^+$ cells was observed, equivalent to 13% at 16 nM I3A and 19% at 250 nM I3A, indicating that active concentrations of residual I3A in crude vector harvest did not increase target cell transduction efficiency.

Furthermore, we demonstrated that enhancement of titer was specific to PKC activation. Transfected cells were pre-treated with the pan-PKC inhibitor bisindolylmaleimide I (BIM-I) or vehicle 1 h prior to induction using NaBu, I3A, or their combination (Figure 1C). NaBu treatment resulted in a 5-fold increase in LV-CMV-GFP titer at harvest with respect to the vehicle control (DMSO), while I3A induced a 6.3-fold increase. The combination of both inducing agents provided the greatest increase in titer,

resulting in a 12.5-fold increase with respect to the vehicle control and a 2.5-fold increase compared to NaBu induction. Notably, pre-treatment of production cells with BIM-I was sufficient to specifically abolish I3A-induced titers without diminishing NaBu-induced LV production. The specificity of this modulation confirmed the distinct induction mechanisms mediated by the two drug classes.

### I3A induces rapid transcription of viral RNA and release of LV particles

The individual and combined effects of NaBu and I3A on LV production kinetics were investigated by assessing changes in titer, cellular vRNA expression, viral structural protein levels, and process quality characteristics throughout the production of LV-CMV-GFP.

Induction with NaBu produced LV via gradual release kinetics, achieving a functional titer of $1.1 \times 10^6$ TU/mL at 8 h post-induction and a maximum titer of $1.0 \times 10^7$ TU/mL at 22 h post-induction (Figure 2A). In contrast, treatment with I3A resulted in a 10-fold increase in the initial rate of LV production, reaching a titer of $1.2 \times 10^7$ TU/mL at 8 h post-induction. When I3A was used alone, the final harvest titer decreased to $6.9 \times 10^6$ TU/mL, likely due to vector degradation and/or loss of infectivity in the later stages of production. However, the combination of I3A and NaBu further enhanced LV production, resulting in a 61% increase in titer between 8 and 22 h and a final titer of $1.9 \times 10^7$ TU/mL. The accelerated initial release of LV particles from production cells was confirmed by an accompanying increase in p24 capsid titer (Figure 2B). Additionally, we observed that LV released within the first 8 h post-I3A induction had a lower particle-to-infectivity (P:I) ratio compared to NaBu-only induction (I3A: $p < 0.001$; NaBu + I3A: $p < 0.05$) (Figure 2C).

A distinct and rapid increase in intracellular vRNA was observed upon PKC activation, with cellular vRNA increasing to 4-fold higher levels compared to NaBu alone 8 h post-induction, as determined by delta-delta RT-qPCR (Figure 2D). Interestingly, intracellular vRNA levels subsequently declined in the absence of NaBu, but continued to increase with the combined induction method to reach 10-fold pre-induction levels. This suggests that the distinct effects of I3A and NaBu on cellular transcription act additively to enhance vRNA levels.

All induction conditions increased the expression of the LV structural proteins Gag precursor (p55) and VSV-G at early and late time points compared to the uninduced control, as determined by western blot (Figures 2E and S2). No substantial differences in total cellular p55 expression were observed at the end of production between the different induction conditions; however, VSV-G envelope expression at final harvest was increased by ~75% when NaBu and I3A were combined compared to NaBu alone (Figures 2F and 2G). Cells were also assessed for transgene (GFP) expression throughout vector production by flow cytometry (Figure 2H). All induction conditions resulted in a higher transgene expression compared to the vehicle control. Induction with I3A alone showed moderately higher levels of transgene expression at the end of production, with 1.4-fold higher GFP expression compared to the NaBu condition ($p < 0.05$).

End-of-production cell viabilities declined to 86%, 83%, and 82% at harvest for NaBu, I3A, and combined induction conditions, respectively, reflecting the relative toxicities of inducing agents on production cells (Figure 2I). Combined addition of I3A and NaBu appeared to significantly reduce cell aggregation with respect to all other conditions (Figure 2J). Cell cycle analysis of end-of-production cells showed that NaBu treatment triggered cell cycle checkpoints and caused an accumulation of cells in $G_2$ phase with a concomitant decrease of cells in S phase (Figure 2K). The relative distribution of cell phases after treatment with I3A alone was similar to the vehicle control.

Residual dsDNA content of the supernatant was broadly equivalent across the conditions 8 h after induction, as measured by PicoGreen assay (Figure 2L). At 22 h post-induction, dsDNA was 30% higher for I3A induction and 80% higher for combined induction with respect to NaBu. Benzonase nuclease treatment was effective at reducing dsDNA content by approximately 2-fold across all tested conditions. Benzonase-treated vector was subsequently purified by Mustang Q anion exchange chromatography and used to transduce activated T cells at matched multiplicities of infection (MOIs 1, 2, and 5) (Figures 2M and 2N). Purified LV from conditions that produced a titer below $1 \times 10^6$ TU/mL were excluded from the T cell transduction assay as material contained insufficient transducing units to achieve an MOI of 1. The transduction efficiency of $CD3^+$ T cells with vector produced under each tested induction condition was equivalent at corresponding MOI, although differences were observed between the two donors due to their varying permissiveness. These results demonstrate that LV infectivity was not compromised by the use of PKC agonist or earlier harvest time points.

### PKC treatment upregulates cellular immediate-early genes during LV production

Changes in the suspension-adapted HEK293T production cell proteome caused by NaBu, I3A, and their combination were assessed by peptide mass spectrometry (Figures 3A–3H). At 22 h post-induction, 131 and 39 differentially expressed proteins ($|\log_2 [FC]| > 1$, $\log_{10}$ [false discovery rate (FDR)] > 1.3) were identified in cells treated with NaBu or I3A, respectively, indicating the comparatively broad influence of HDAC inhibition on the production cell proteome (Figures 3D and 3E). Combined NaBu and I3A dosing resulted in substantial dysregulation of protein expression, with 342 host cell proteins identified as being differentially expressed at the final time point (Figure 3F). A large overlap of differentially expressed proteins induced by HDAC inhibition were common to both individual and combined treatment groups (105 proteins), which included upregulation of LGALS1, PCDH9, and HIST1H1T, and downregulation of ZIC2, SPON1, and GFRA2 (Figure S3).

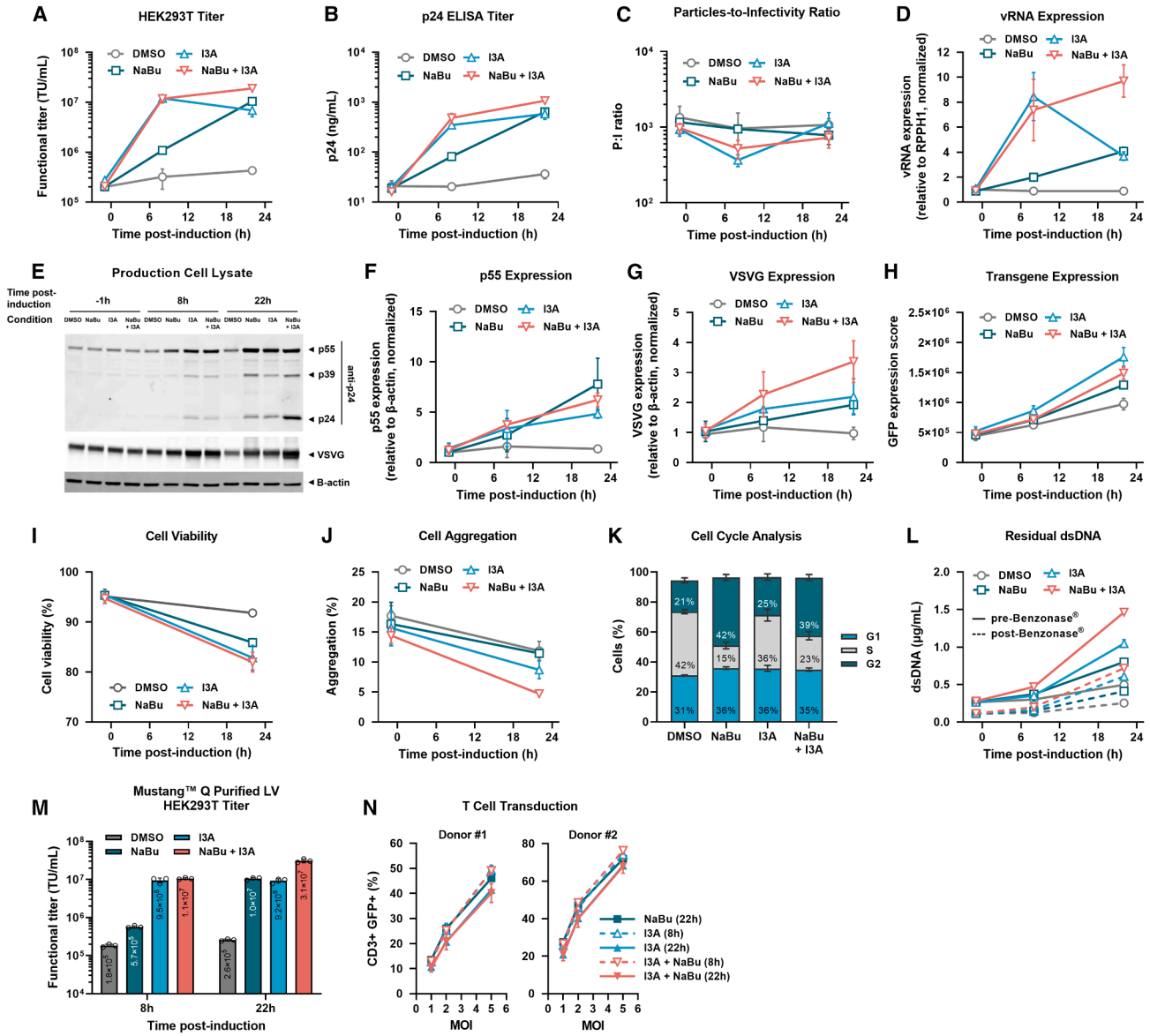


**Figure 2. Time course analysis of LV-CMV-GFP production in suspension-adapted HEK293T**

(A) Functional LV titer produced using the following induction conditions: 0.2% (v/v) DMSO (gray), 10 mM NaBu + 0.2% (v/v) DMSO (green), 250 nM I3A (blue), and 10 mM NaBu + 250 nM I3A (red). (B) HIV p24 capsid quantification measured by p24 ELISA. (C) Particle-to-infectivity ratio derived from functional titer and physical viral particles. (D) Cellular vRNA expression relative to RPPH1 mRNA determined by RT-qPCR and normalized to pre-induction values. (E) Representative western blot showing cellular expression of viral structural proteins using anti-p24 and anti-VSV-G antibodies. Gag-Pol cleavage products: p55 (Gag precursor), p39 (matrix-capsid), p24 (capsid), and envelope protein VSV-G are indicated. β-actin was used as loading control. (F and G) Changes in cellular expression of (F) p55 and (G) VSV-G relative to β-actin and normalized to pre-induction values, as determined by quantification of western blot in (E) and Figure S2. (H) Transgene protein expression level in production cells measured by flow cytometry. (I and J) Viability (I) and aggregation (J) of production cells. (K) Cell cycle analysis of end-of-production cells showing percentage of cells in $G_1$ (blue), S (gray), and $G_2$ (green). (L) Residual dsDNA in vector harvest measured using a PicoGreen assay showing pre-Benzonase- (solid lines) and post-Benzonase-treated (dashed lines) cell culture supernatant. (M) Functional titer of Benzonase-treated Mustang Q purified LV determined by flow cytometry of HEK293T cells three days post-transduction. (N) Transduction efficiency of T cells from two donors determined by flow cytometry 5 days post-transduction at MOIs 1, 2, and 5. All data are mean average values ± SD of biological triplicates ($n$ = 3).

PKC stimulation by I3A resulted in a rapid and prominent expression of cellular immediate-early genes within 8 h of treatment, including a sustained upregulation of AP-1 transcription factor subunit, JUNB, and early growth response factor, EGR1.[32] Graphing of differentially expressed proteins by known functional and physical associations using the STRING[33] database (version 12.0) highlighted

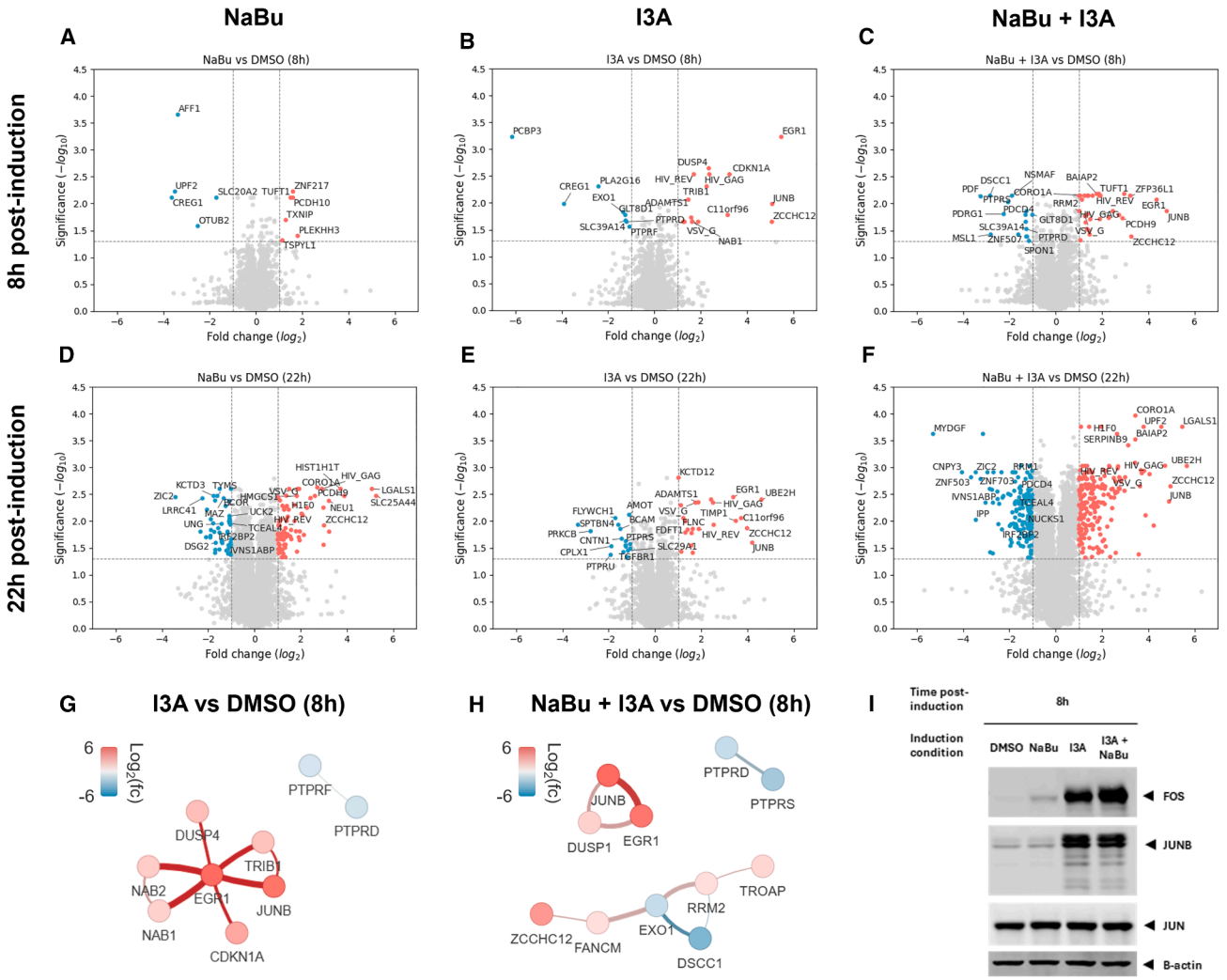


**Figure 3. PKC treatment upregulates cellular immediate-early genes during LV production**

(A–F) Label-free quantitative peptide mass spectrometry of suspension-adapted HEK293T during production of LV-CMV-GFP. Volcano plots showing differentially expressed proteins in production cells collected 8 h (top) and 22 h (bottom) after treatment with 10 mM NaBu + 0.2% (v/v) DMSO (left), 250 nM I3A (middle), or 10 mM NaBu + 250 nM I3A (right). Changes are shown with respect to vehicle (0.2% [v/v] DMSO)-treated cells collected at the same respective time points. Highlighted proteins are shown with $|\log_2 (FC)| > 1$ and $-\log_{10} (FDR) > 1.3$ ($n = 3$). (G and H) STRING network association graphs of up- (red) and downregulated (blue) human proteins in production cell pellets 8 h after induction with (G) I3A and (H) NaBu + I3A. Protein candidates were selected on basis of $|\log_2 (FC)| > 1$ and $-\log_{10} (FDR) > 1.3$ (19 and 41 protein candidates, respectively). Node color illustrates fold change with respect to DMSO-treated cells, and line thickness illustrates confidence of supporting data (interaction score cut-off >0.4). (I) Western blot probing for cellular expression of AP-1 proteins JUN, JUNB, and FOS at 8 h post-induction with 0.2% (v/v) DMSO, 10 mM NaBu + 0.2% (v/v) DMSO, 250 nM I3A, or 10 mM NaBu + 250 nM I3A ($n = 1$).

the strength of the JUNB/EGR1 axis in the immediate cellular response to PKC activation for both treatment groups. However, no significant protein-protein associations were observed for the NaBu treatment group at the equivalent time point (Figures 3G and 3H). PKC-induced upregulation of the transcriptional repressor proteins, NAB1 and NAB2, was consistent with response to EGR1 transcription.[34] Upregulation of the dual specificity protein phosphatase DUSP4 was indicative of feedback regulation of ERK-mediated phosphorylation.[35] A distinct PKC-induced expression of AP-1 subunits, JUNB and FOS, was confirmed by western blot of cell lysate 8 h post-induction, whereas JUN appeared to be constitutively expressed and unaffected by induction condition (Figure 3I).

### PKC activation induces the production of therapeutic LV-CAR and synergizes with a modified U1 snRNA-based LV enhancer to increase titers

The individual and combined effects of NaBu and I3A were assessed in the small-scale production of a therapeutic LV. The transgene for a therapeutic CAR targeting the tumor-associated antigen 5T4 (CAR.5T4) with an internal EF1α promoter was selected as an

example of a product that is known to yield comparatively low titers under standard conditions. LV with a GFP transgene (and otherwise identical cassette sequences) was produced in parallel to directly compare the influence of induction conditions across the different transgenes. In addition, vector was produced with and without co-expression of modified U1 snRNA "256U1."[20,21]

LV-EF1α-CAR.5T4 yielded 7.5-fold lower integrating titers compared to LV-EF1α-GFP under NaBu induction conditions ($1.6 \times 10^6$ TU/mL vs. $1.2 \times 10^7$ TU/mL). Interestingly, we observed that the relative fold change induced by I3A compared to NaBu differed between the two vector products (Figures 4A–4D and S4). Induction with I3A or NaBu induced equivalent titers of LV-EF1α-GFP ($1.2 \times 10^7$ TU/mL), whereas I3A induced a 3.6-fold increase in LV-EF1α-CAR.5T4 titer compared to NaBu alone ($5.8 \times 10^6$ TU/mL vs. $1.6 \times 10^6$ TU/mL). Conversely, combined dosing with NaBu and I3A increased titers of LV-EF1α-GFP by 3-fold with respect to NaBu ($3.7 \times 10^7$ TU/mL vs. $1.2 \times 10^7$ TU/mL), whereas no further increase in titer of LV-EF1α-CAR.5T4 was achieved.

Significant improvements in titer were observed across all conditions where 256U1 was co-transfected alongside packaging plasmids. Co-expression of 256U1 increased titers of LV-EF1α-GFP and LV-EF1α-CAR.5T4 produced under NaBu induction by 2.9- and 4.9-fold, respectively. When 256U1 was co-expressed together with combined induction using I3A and NaBu, a respective 5.2- and 8.8-fold increase in integrating titer was achieved for LV-EF1α-GFP and LV-EF1α-CAR.5T4 compared to standard 3$^{rd}$ generation conditions. PKC agonist had no detrimental impact on the P:I ratio of either vector product (Figures 4E and 4F).

### Identification of kinases activated by PKC agonists and their downstream substrates

Phosphopeptide mass spectrometry was used to identify the kinases activated by PKC agonists and their downstream substrates in HEK293T-derived production cells. Induction with NaBu and prostratin resulted in a 2.9-fold increase in LV-EF1α-CAR.5T4 functional titers compare to NaBu (Figure 5A). The p24 capsid titer at harvest increased by 2.2-fold ($p < 0.001$) and a 24% decrease in P:I ratio was observed ($p < 0.05$) (Figure S5). A total of 422, 645, and 411 differentially phosphorylated peptides ($|\log_2 (FC)| > 3$ and $\log_{10} (FDR) > 1.3$) were detected at 10, 60, and 360 min following treatment with PKC agonist, respectively (Figures 5B–5D). The immediate response to PKC activation was characterized by pronounced phosphorylation of SMC4 (S28), BCL7C (S122), and CTTN (T399/S405) and dephosphorylation of SETD2 (S2080/S2082), SPTAN1 (S1031), and ZNF318 (S40) (Figure 5B). Activation of the mitogen-activated protein kinase (MAPK) pathway was directly observed through phosphorylation of MAPK1 (ERK2) at T187 and MAPK3 (ERK1) at T203. A total of 61 phosphosites were detected as being constitutively changed at all collected time points, including phosphorylation RPS6KA1 at T359/S363 and dephosphorylation of LARP4B at T732 (Figure S6).

Gene ontology (GO) enrichment of phosphorylated substrate was performed using Enrichr.[36] GO biological process analysis highlighted strong enrichment of phosphorylated proteins involved in "positive regulation of GTPase activity," "endosomal transport," and "vesicle-mediated transport," which was particularly pronounced at 60 min post-induction (Figure 5E). GO molecular function analysis revealed a high enrichment of phosphorylated species involved in "cadherin binding," "GTPase regulator activity," and "RNA binding" (Figure 5F).

Kinase substrate enrichment analysis (KSEA) was performed using the method described by Wiredja et al.[37] KSEA confirmed a strong enrichment of phosphorylated substrate associated with diacylglycerol signaling, revealing high constitutive activity of the classic PKC isoform, PKCα (PRKCA); calcium-independent isoforms, PKCε (PRKCE) and PKCδ (PRKCD); and the C1-domain containing kinase PKD1 (PRKD1) (Figure 5G). Activity of the MAPK pathway was characterized by positive enrichment of substrate associated with MEK1/2 (MAP2K1/2) and ERK1/2 (MAPK3/1), and downstream kinases, including p70 ribosomal S6 kinase (RPS6KB1) and MAPK activated protein kinase 2 (MAPKAPK2). KSEA highlighted a strong initial downregulation of the activity of cyclin dependent kinases 2 and glycogen synthase kinase 3 beta, and strong downregulation of mammalian target of rapamycin activity at the final time point.

Differentially phosphorylated proteins ($|\log_2 (FC)| > 5$ and $\log_{10} (FDR) > 1.3$) from all three time points were collated and analyzed using the MetaScape Web App[38] to identify enriched phosphoprotein complexes (Figure 5H). Proteins associated with transcription and formation of the elongation complex were highlighted, including RNA polymerase II (POLR2A; S1913$^{P-}$/S1927$^{P-}$); the nucleosome remodeling and deacetylase (NuRD) complex member CHD4 (T703$^{P+}$); and elongation factors IWS1 (S248$^{P+}$/S250$^{P+}$/S252$^{P+}$/S261$^{P+}$), EAF (T157$^{P+}$), ELL (S309$^{P-}$), and NELFE (S51$^{P+}$). A distinct cluster of proteins was identified associated with nucleocytoplasmic transport of mRNA and pre-mRNA processing (TPR [T2137$^{P+}$], NUP153 [S516$^{P+}$], NUP188 [T1712$^{P+}$], RANBP2 [S1869$^{P+}$], NCBP1 [S22$^{P+}$], SRRM1 [S426$^{P+}$/S431$^{P+}$], SRSF11 [S207$^{P+}$/S212$^{P+}$], SRSF5 [S231$^{P+}$/S233$^{P+}$], POLDIP3 [S383$^{P+}$], and ZC3H11A [S758$^{P+}$/S759$^{P+}$]). Furthermore, a cluster of proteins involved in translation were identified, including EIF4G1 (T1073$^{P-}$), EIF4G2 (T508$^{P+}$), and EIF3B (S83$^{P+}$/S85$^{P+}$).

### LV production induced by PKC agonist is independent of NF-κB activation

Phosphorylation of NF-κB modulators by IκB kinase (IKK) was not detected in the phosphoproteome after PKC activation (Figure 5G). To further investigate if NF-κB transcriptional activity was activated by PKC stimulation in HEK293T production cells, a luciferase reporter assay was performed. No change in NF-κB activity was observed following stimulation with I3A (or NaBu) when cells were co-transfected with a luciferase reporter containing a tandem NF-κB response element (Figure 6A). In contrast, a ∼300-fold

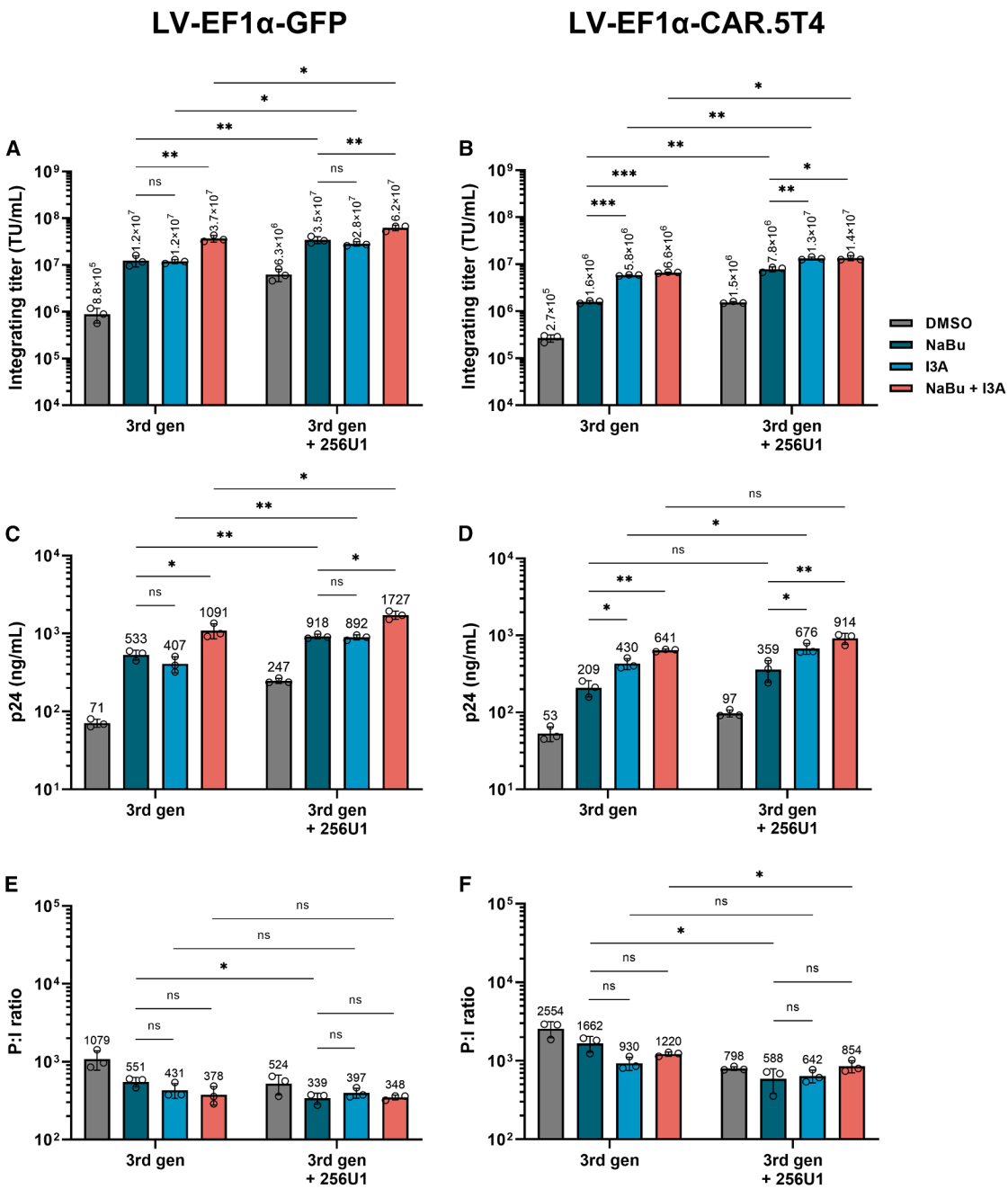


**Figure 4. PKC activation induces the production of therapeutic CAR LV and synergizes with a modified U1 snRNA-based LV enhancer to increase titers**

(A and B) Integrating titer of (A) LV-EF1α-GFP and (B) LV-EF1α-CAR.5T4 harvested 23 h post-induction. LV was produced in suspension-adapted HEK293T using 3rd generation LV plasmids ± co-transfection with a plasmid coding for the retargeted U1 snRNA enhancer "256U1." The following conditions were used for induction: 0.2% (v/v) DMSO (gray), 10 mM NaBu + 0.2% (v/v) DMSO (green), 250 nM I3A (blue), and 10 mM NaBu + 250 nM I3A (red). Integrating titers were determined by duplex qPCR assay probing for Ψ and RPPH1 10 days post-transduction of HEK293T cells. (C and D) HIV p24 capsid titer of (C) LV-EF1α-GFP and (D) LV-EF1α-CAR.5T4 measured by p24 ELISA. (E and F) Particle-to-infectivity ratio of (E) LV-EF1α-GFP and (F) LV-EF1α-CAR.5T4 derived from integrating titer and physical virus particles. Statistical significance was established using Welch's t test: *$p < 0.05$, **$p < 0.01$, and ***$p < 0.001$; ns, not significant. All data are mean average values ± SD of biological triplicates ($n = 3$).

induction of luciferase activity was observed following treatment of cells with the NF-κB activator, tumor necrosis factor alpha (TNF-α). Interestingly, we found that NF-κB stimulation with TNF-α was sufficient to induce a 3-fold increase in LV-CMV-GFP titer with respect to the PBS control. We then asked whether stimulating NF-κB pathways would be sufficient to further enhance LV

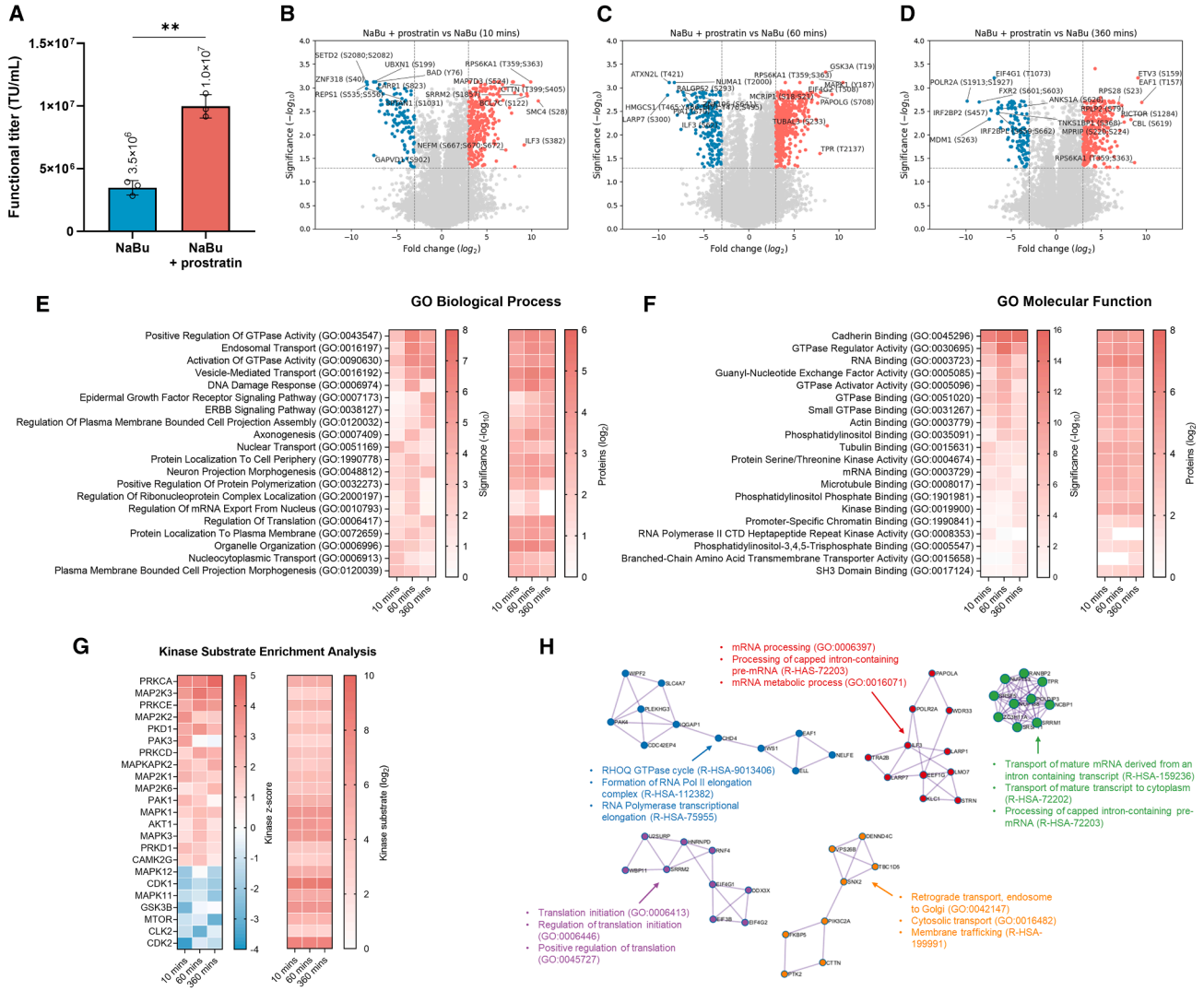


**Figure 5. Phosphopeptide mass spectrometry of suspension-adapted HEK293T during production of LV-EF1α-CAR.5T4**

(A) Functional titer of LV-EF1α-CAR.5T4 harvested 24 h after induction with 10 mM NaBu + 0.2% (v/v) DMSO (blue) or 10 mM NaBu + 10 μM prostratin (red). LV was produced in suspension-adapted HEK293T transfected with 3rd generation LV plasmids and retargeted U1 snRNA enhancer "256U1." Data are mean average values ± SD of biological triplicates ($n = 3$). Statistical significance was established using Welch's t test: $^{**}p < 0.01$. (B–D) Volcano plots showing differentially phosphorylated proteins (B) 10 min, (C) 60 min, and (D) 360 min after treatment with NaBu + prostratin. Changes are shown with respect to NaBu + DMSO treated cells collected at the same respective time points. Highlighted phosphorylation sites are shown with $|\log_2(FC)| > 3$ and $\log_{10}(FDR) > 1.3$ ($n = 3$). (E and F) (E) GO biological process and (F) GO molecular function enrichment analysis of phosphorylated protein candidates ($|\log_2(FC)| > 3$ and $-\log_{10}(FDR) > 1.3$) showing top 20 significantly enriched terms (left) and number of proteins detected for each term (right). (G) Kinase substrate enrichment analysis showing kinase $Z$ score (left) and corresponding number of identified kinase substrates (right). Analysis was performed using PhosphoSitePlus and NetworKIN datasets with $p$ value <0.05 and substrate count >5. Kinases with a $|Z$ score$| > 2$ at one or more time points are shown. (H) Protein-protein interaction enrichment analysis of differentially phosphorylated protein ($|\log_2(FC)| > 5$ and $-\log_{10}(FDR) > 1.3$) collated from all collected time points (264 total protein candidates) using the Metascape Webb App with the following databases: STRING, BioGrid, OmniPath, and InWeb_IM. The molecular complex detection (MCODE) algorithm has been applied to identify densely connected network components. Pathway and process enrichment analysis has been applied to each MCODE component independently, and the three best-scoring terms by $p$ value have been retained as the functional description of the corresponding components.

expression alongside HDAC inhibition and/or PKC activation (Figure 6B). Titers were increased 1.9- and 2.6-fold when TNF-α was combined with NaBu or I3A, respectively. However, no significant improvement was observed upon stimulation with TNF-α in addition to combined NaBu and I3A treatment.

## DISCUSSION

Over the last 30 years, the viral vector bioprocessing field has empirically identified HEK293T cells as one of the most productive to date. This mainly relates to their high transfection efficiency and negligible expression of relevant virus restriction factors.[8,39–41] However, viral

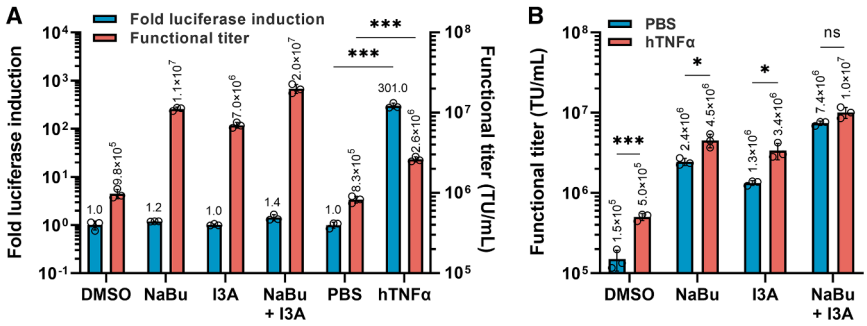


**Figure 6. LV production induced by PKC agonist is independent of NF-κB activation**

(A) Fold change in NanoLuc NF-κB response element luciferase activity during production of LV-CMV-GFP in suspension-adapted HEK293T (blue, left axis). Luciferase activity was measured 5 h after stimulation of cells with 0.2% (v/v) DMSO, 10 mM NaBu + 0.2% (v/v) DMSO, 250 nM I3A, 10 mM NaBu + 250 nM I3A, PBS, or 20 ng/mL hTNF-α. Corresponding functional titers of LV harvested 22 h post-induction are shown (red, right axis). (B) Functional titers of LV-CMV-GFP harvested 22 h post-induction with 0.2% (v/v) DMSO, 10 mM NaBu + 0.2% (v/v) DMSO, 250 nM I3A, or 10 mM NaBu + 250 nM I3A. All conditions were treated with 20 ng/mL hTNF-α (red) or PBS (blue) immediately after induction. Functional LV titers were determined by flow cytometry of HEK293T three days post-transduction. Statistical significance was established using Welch's t test: *$p < 0.05$ and ***$p < 0.001$; ns, not significant. All data are mean average values ± SD of biological triplicates ($n = 3$).

vectors are susceptible to significant transcriptional suppression that results in suboptimal titers, often alleviated by the addition of HDAC inhibitors such as sodium butyrate.[4,11,13,42] Here, our results identify PKC agonists as a class of inducing agents that complement the use of sodium butyrate to enhance the manufacture of therapeutic HIV-1-based LV.

Our evaluation of the interaction between sodium butyrate and I3A revealed that combined dosing improved titers of a GFP reporter LV by ∼2-fold compared to HDAC inhibitor alone. This was characterized by rapid transcription of vRNA and release of p24 capsid, and without detriment to particle-to-infectivity ratio or T cell transduction efficiency of vector product. Furthermore, combined dosing was well tolerated by production cells despite having a pleiotropic impact on cellular protein expression. Interestingly, we observed that high initial PKC-induced vRNA levels were sustained in the presence of sodium butyrate, indicating a cooperative effect resulting from the drug combination that promotes elevated and stable levels of cellular vRNA.

We have also shown that PKC agonists are superior to sodium butyrate in the production of a therapeutic CAR vector (LV-EF1α-CAR.5T4), resulting in a ∼3-fold increase in titer. Furthermore, increases in LV titers were observed across all inducing conditions in the context of co-expression of the "256U1" LV enhancer, which acts downstream of transcription initiation to increase availability of full-length vRNA.[20,21] The cumulative benefit of these technologies was demonstrated by a ∼9-fold increase in titer of LV-EF1α-CAR.5T4 compared to our standard 3$^{rd}$ generation process. Taken together, these results emphasize the productivity improvements that can be achieved by maximizing vRNA availability in LV production.

The broad phosphoproteome signature of PKC activation during LV production was consistent with activation of PKCα, δ, and ε isoforms and the MAPK pathway. We also observed a prominent upregulation of cellular immediate-early genes associated with the MAPK cascade, including as EGR1 and DUSP4.[34,35,43] Of particular interest was the distinct upregulation of AP-1 subunits FOS and JUNB, which provide an association between transcription factors engaged downstream of PKC/MAPK activation and the single TPA-responsive element (5′-TGA(G/C)TCA-3′) present in the CMV immediate-early (IE) promoter.[18,44–46]

PKC activation is often linked to stimulation of NF-κB signaling pathways, which trigger the transcription of genes involved in antiviral defenses and inflammation.[8,47–49] Viruses harboring NF-κB sites in their promoter region exploit this pathway to enhance viral gene transcription and directly regulate their replication cycle.[50] Interestingly, we did not observe evidence of PKC-induced NF-κB activity via characteristic phosphorylation by the signaling intermediate IKK, nor did we observe NF-κB transcriptional activity via luciferase reporter assay. This leads us to conclude that PKC-stimulated LV transcription in our HEK293T-based production cells is independent of the classic NF-κB pathway.[49] Indeed, stimulation of production cells with the NF-κB activator TNF-α was sufficient to induce a further increase of LV titer when combined with I3A, which suggests that concerted engagement between AP-1 and NF-κB transcription factors and the CMV-IE promoter can be achieved when these pathways are simultaneously activated, albeit via distinct stimuli.

In addition to AP-1 upregulation, pronounced changes to the phosphorylation state of proteins that modulate transcription and chromatin remodeling were identified. Notably, changes to the phosphorylation state of the C-terminal domain of the large subunit of RNA polymerase II and elongation factors align with the complex and dynamic events that lead to transcription initiation and progression.[51] Furthermore, changes to phosphorylation of histone modifying proteins, such as the histone methyltransferase SETD2 and the NuRD complex member CHD4, indicates that proteins involved in epigenetic restriction constitute downstream effectors of PKC activation.[49,52,53] Taken alongside changes to the phosphorylation state of proteins involved in RNA binding, splicing, and export, it is plausible that numerous concerted processes are involved in enhancing episomal LV gene expression and vRNA availability following PKC activation.[49]

The commercial case for the use of I3A within LV manufacturing is supported by the relatively low dose required for induction, the ease

of its incorporation within existing manufacturing processes, and its historic GMP-grade manufacture for clinical use.[31] An in-house high-performance liquid chromatography assay has demonstrated to us that soluble I3A has a storage stability >8 months in solution and is effectively cleared from vector product following anion exchange chromatography (data not shown). Furthermore, its application is compatible with in-house technologies to improve LV production, including 256U1 (as shown here) and the transgene repression in production system[9] (data not shown). From a bioprocessing perspective, the increased rate of release of LV particles may present further advantages, wherein harvesting LV at an earlier time point reduces exposure of LV product to the bioreactor environment, while also reducing the residual DNA and protein burden carried through to downstream processing. Building on the understanding of our LV production system outlined here, we will further explore I3A as an induction enhancer with the aim of reducing the cost of manufacturing LV-based therapies.

## MATERIALS AND METHODS

### Lentiviral vector production

LV was produced using suspension-adapted HEK293T cells (derived from an adherent HEK293T GMP cell bank) in FreeStyle 293 media (12338018, Gibco) supplemented with 0.1% cholesterol lipid concentrate (12531018, Invitrogen) in vented 125 mL Erlenmeyer shake flasks (431143, Corning) or 24-deep well plates (P-DW-10ML24C, Corning). Cells were maintained at 37°C and 5% $CO_2$ on an orbital shaker rotating at 200 rpm throughout incubation. Approximately 24 h after seeding, cells were transfected with 3rd generation LV plasmids (0.95 μg/mL genome, 0.1 μg/mL Gag-Pol, 0.07 μg/mL VSV-G, and 0.06 μg/mL Rev) using Lipofectamine 2000CD (12566014, Invitrogen). HIV-1 LV genomes and packaging plasmids have been described previously, and all used CMV promoters.[54–56] Where indicated, 0.2 μg/mL plasmid encoding a retargeted U1 snRNA (256U1) enhancer was co-transfected with 3rd generation LV plasmids.[20,21] Cells were induced using sodium butyrate (1371270250, Merck), I3A (SML1318, Merck), prostratin (P0077, Merck), bryostatin (B7431, Merck), and phorbol 13-myristate acetate (524400, Merck) at stated concentrations 16–20 h after transfection. Control conditions were treated with an equivalent volume (0.2% v/v) of DMSO (D2438, Merck). For PKC inhibition experiments, 2 μM BIM-I (203290, Merck) or 0.1% (v/v) DMSO was added to production cells 1 h prior to the addition of inducing agents. Cell culture media was not replaced during vector production experiments. Cell viability was monitored using a Nucleocounter NC-202 (Chemometec). Transgene expression of cells was measured using an Attune NxT (Thermo Fisher Scientific) and the transgene expression score was determined using Equation 1. End-of-production cells were washed with PBS and vector-containing supernatant was 0.45 μm filtered prior to storage at −80°C for subsequent analysis.

$$\textit{expression score} = \textit{transgene postive cells}\ (\%) \times \textit{geometric mean fluorescence intensity} \quad \text{(Equation 1)}$$

### Functional titer determination by flow cytometry

Tissue culture-treated 96-well flat-bottom plates (353072, Corning) were seeded with $1.0 \times 10^4$ adherent HEK293T cells/well in 100 μL Dulbecco's Modified Eagle's Medium (DMEM) (D6429, Merck) supplemented with 10% fetal bovine serum, 1× MEM non-essential amino acids (M7145, Merck), and 4 mM L-glutamine (G7513, Merck). Media was removed after 24 h and replaced with 55 μL/well vector dilution in complete DMEM supplemented with 8 μg/mL polybrene (TR-1003-G, Merck). Wells were topped up with 150 μL complete DMEM 3–6 h post-transduction and incubated for three days at 37°C and 5% $CO_2$. Cells were resuspended using TrypLE Express (12605010, Gibco) for analysis by flow cytometry. CAR.5T4-expressing cells were stained using Alexa Fluor 594 F(ab')2-goat anti-mouse IgG (H + L) (115-586-072, Jackson ImmunoResearch) diluted in BSA Stain Buffer (554657, BD Biosciences) supplemented with 5% goat serum (G9023, Merck). Flow cytometry was performed on an Attune NxT (Thermo Fisher Scientific) gated to collect 10,000 events on the single cell population. Functional titers were determined using Equation 2.

$$\textit{Functional Titer}\left(\frac{TU}{mL}\right) = \frac{-\ln\left(1 - \frac{\textit{transduced cells}\ (\%)}{100}\right) \times \textit{cells at transduction} \times \textit{dilution factor}}{\textit{volume diluted vector}\ (mL)} \quad \text{(Equation 2)}$$

### Nuclease treatment and anion exchange chromatography

Where stated, filtered vector harvest was treated with 25 U/mL Benzonase nuclease with 2 mM $MgCl_2$ for 1 h at 37°C. A Mustang Q AcroPrep Advance 96-well (8171, Cytiva) plate was equilibrated using wash buffer (20 mM Tris, 2 mM $MgCl_2$, 0.15 M NaCl, pH 7.2) prior to loading 1 mL clarified vector with negative pressure generated using a vacuum pump. Membrane was washed with 64 membrane volumes of wash buffer before applying 18 membrane volumes elution buffer (20 mM Tris, 2 mM $MgCl_2$, 1.2 M NaCl, pH 7.2). Eluted vector was equilibrated to final formulation of 20 mM Tris, 0.15 M NaCl, 1% sucrose, 1% mannitol, pH 7.2.

### T cell transductions

Donor peripheral blood mononuclear cells (PBMCs) were activated on the day of thawing using Dynabeads Human T-Activator CD3/CD28 for T Cell Expansion and Activation (11161D, Gibco) at a 1:1

bead-to-cell ratio in X-Vivo 15 media (BEBP02-061Q, Lonza) supplemented with Human AB Serum (H5667, Merck), MEM Eagle Vitamins (25-020-CI, Corning), GlutaMax (35050061, Gibco), HEPES (15630056, Gibco), sodium pyruvate (S8636, Merck), IL-7 (130-095-363, Miltenyi Biotec), and IL-15 (130-095-765, Miltenyi Biotec). Activated cells were incubated for 48 h prior to transduction. Magnetic activation beads were removed on the day of transduction and T cells were resuspended in fresh complete media. T cells were seeded in a 96-well U-bottom plate (353077, Corning) with a seeding density of $1 \times 10^5$ cells/well in 100 μL media. Vector dilutions were prepared in complete media, and 100 μL diluted vector was added directly to plated T cells. Final vector concentrations were $5 \times 10^5$ TU/mL, $1 \times 10^6$ TU/mL, and $2.5 \times 10^6$ TU/mL at MOIs 1, 2, and 5, respectively, with a final well volume of 200 μL. Nevirapine (SML0097, Merck) controls were included for transductions at MOI 5. Cells were stained for flow cytometry 5 days post-transduction with Zombie NIR Fixable Viability Dye (423105, BioLegend), BUV395 mouse anti-human CD3 (564001, BioLegend), BV421 mouse anti-human CD4 (566703, BioLegend), and PE anti-human CD8 Antibody (344706, BioLegend). Flow cytometry was performed on a LSRFortessa X-20 (BD Biosciences) gated to collect 20,000 events on the live cell population.

#### Cell cycle analysis

End-of-production cells were fixed and permeabilized in ice-cold 70% ethanol for 1 h at 4°C prior to washing with PBS. Cells were treated using RNase A and stained for analysis using propidium iodide according to kit instructions (ab139418, Abcam). Cells were analyzed by flow cytometry using an Attune NxT (Thermo Fisher Scientific) gated to collect 100,000 events on the single cell population. The Watson method was used to determine the relative proportions of cells in each cell cycle phase in FlowJo software (version 10.9.0, BD Biosciences).

#### Delta-delta RT-qPCR

Total cytoplasmic RNA was extracted from cell pellets using a QIAamp Viral RNA Mini Kit (52904, QIAGEN). DNA was subsequently removed using a DNA-free DNA Removal Kit (AM1906, Invitrogen) according to kit instructions. RT-qPCR was performed using a QuantStudio 7 (Thermo Fisher Scientific) under standard chemistry RT-PCR cycling conditions using TaqMan Fast Virus One-Step Master Mix (4444436, Thermo Fisher Scientific) and primer-FAM-probe sets against HIV-1 packaging signal (Ψ) or housekeeping gene ribonuclease P RNA component H1 (RPPH1). Negative RT controls were included for both reaction sets. The following primer/probe sequences were used.

Ψ-forward: 5′-TGGGCAAGCAGGGAGCTA-3′

Ψ-reverse: 5′-TCCTGTCTGAAGGGATGGTTGT-3′

Ψ-probe: 5′-FAM-AACGATTCGCAGTTAATCCTGGCCTGTT-TAMRA-3′

RPPH1-forward: 5′-CCCTAGTCTCAGACCTTCCCAAG-3′

RPPH1-reverse: 5′-GCGGAGGGAAGCTCATCAG-3′

RPPH1-probe: 5′-VIC-CCACGAGCTGAGTGCGTCCTGTCA-TAMRA-3′.

#### p24 capsid quantitation

HIV-1 p24 capsid quantification was performed using an Alliance HIV-1 p24 ELISA kit (NEK050001, PerkinElmer) according to kit instructions. Absorption was measured using a SpectraMax i3X (Molecular Devices) at 490 nm. Physical LV particles were calculated assuming 2,000 molecules of p24 per viral capsid.

#### Western blots

Cell lysate was prepared in 1× RIPA lysis buffer (20–188, Millipore) and total protein concentration determined using a Pierce BCA Protein Assay Kit (23225, Thermo Fisher Scientific). Proteins were separated using SDS-PAGE under reducing conditions in a 4–20% Criterion TGX 26-well pre-cast gel (5678095, Bio-Rad). Western transfer to a nitrocellulose membrane was carried out using a Trans-Blot Turbo system (Bio-Rad). Membranes were probed with primary antibodies for p24 (ab32352, Abcam), VSV-G (PA1-30138, Invitrogen), c-Jun (9165T, Cell Signaling Technologies), JunB (3753T, Cell Signaling Technologies), c-Fos (2250T, Cell Signaling Technologies) or β-actin (ab8226, Abcam). Membranes were incubated with StarBright 700 α-Rb and StarBright 520 α-Ms secondary antibodies and imaged using a ChemiDoc Imager (Bio-Rad). Where applicable, band intensities were quantified using Image Lab software (version 6.0.1, Bio-Rad).

#### Residual DNA quantification

Residual DNA was quantified using a Quant-iT PicoGreen dsDNA kit (P7589, Thermo Fisher Scientific) according to kit instructions. Fluorescence emission was measured with a SpectraMax i3X (Molecular Devices) with an excitation wavelength of 485 nm and emission wavelength of 538 nm.

#### Integrating titer determination by duplex qPCR

Tissue culture-treated 48-well flat-bottom plates (353078, Corning) were seeded with $2 \times 10^4$ adherent HEK293T cells/well. Transductions were performed as per the functional titer assay with 100 μL/well vector dilution and 200 μL complete DMEM top-up. Untransduced cells were included as a negative control for vector integration. HEK293T cells were serially passaged 3 times over the course of 10 days following transduction. Cells were harvested at assay termination and genomic DNA was extracted using a QIAamp 96 DNA QIAcube HT kit (51331, QIAGEN) according to kit protocol using a QIAcube HT (QIAGEN). Extracted DNA was used as template for duplex TaqMan qPCR reactions using TaqMan Gene Expression Master Mix (4369016, Thermo Fisher Scientific) and primer-FAM-probe sets against Ψ and primer-VIC-probe sets against RPPH1 (described previously). Reactions were performed under standard chemistry PCR cycling conditions using a QuantStudio 7 (Thermo Fisher Scientific). Single integrant reference control DNA (1 copy Ψ per HEK293T cell) was used to derive cells per reaction. Integrating vector titers were determined using Equation 3.

$$Integrating\ Titer\left(\frac{TU}{mL}\right) = \frac{\frac{\Psi\ copies}{cell} \times cells\ at\ transduction \times dilution\ factor}{volume\ diluted\ vector\ (mL)} \quad \text{(Equation 3)}$$

## Proteomics

### Sample preparation

Cell lysates were prepared in 1% (v/v) SDS and 50 mM ammonium bicarbonate prior to incubating at 70°C for 10 min. DNA was sheared by sonication. Samples were reduced with 5 mM dithiothreitol at 70°C for 10 min and alkylated with 15 mM iodoacetamide in the dark at room temperature for 30 min. SP3 workflow was followed for protein cleanup using Sera-Mag Speed beads (Cytiva) followed by trypsin-LysC digestion overnight. Per sample, 0.5% (v/v) trifluoracetic acid was added, and samples were cleaned up using C18 SPE cartridge (Thermo Fisher Scientific) and eluted using 50% (v/v) acetonitrile. Eluted peptide was dried using SpeedVac system and resuspended in 0.1% formic acid.

### LC-MS/MS acquisition

All data were acquired using a Vanquish Neo LC system (Thermo Fisher Scientific) coupled to an Orbitrap Exploris 480 mass spectrometer with an FAIMS Pro Duo module operating in data-independent acquisition (DIA) mode. An Easy-Spray PepMap Neo analytical column (75 μm × 500 mm, 2 μm particle) (ES75500PN; Thermo Fisher Scientific) was used at 300 nL/min flow rate. Eluting peptides were sprayed into the mass spectrometer at 1,800 V while FAIMS CV was kept at −55°C and carrier gas flow was set at 4.0 mL/min. RF lens was kept at 40%.

### Data processing

Data were processed by Spectronaut (version 18, Biognosys) using a UniProt Human FASTA database. Mass spectrometry data were filtered to contain only protein hits present in all 3 replicates of at least one treatment group. Missing data were imputed using random draws from a Gaussian distribution centered around a minimal value (0.01 quantile) with a standard deviation estimated as the median protein-wise standard deviation. $p$ values were determined using a two-sample Student's t test and adjusted for false discovery rate of 0.05 using the Benjamini-Hochberg procedure.

## Phosphopeptide proteomics

### Sample preparation and phosphopeptide enrichment

Phosphopeptide mass spectrometry was performed by Biognosys AG (Switzerland). Cell pellets were lysed and denatured using Biognosys' Denature Buffer and treated with Benzonase. Protein concentrations were determined using a BCA assay (Thermo Fisher Scientific). Per sample, 1.5 mg of protein mass were reduced/alkylated using Biongosys Reduction/Alkylation Solution for 1 h at 37°C and digested overnight at 37°C using trypsin at a protein:protease ratio of 50:1. Digested samples were desalted using an Oasis HLB 96-well plate 30 μm (30 mg) (Waters) according to the manufacturer's instructions and dried down using a SpeedVac system. Peptides were resuspended in Sol A (1% acetonitrile and 0.1% formic acid). Peptide concentrations were determined using a ultraviolet-visible spectrometer at 280 nm (SPECTROstar Nano, BMG Labtech). Per sample, 500 μg of peptide mass were phospho-enriched using Ti IMAC HP beads (MagReSyn) on a KingFisher. Flex system (Thermo Fisher Scientific)-enriched samples were desalted as before on an Oasis HLB μElution plate 30 μm (Waters). Dried samples were resolved in 21 μL of Sol A and spiked with Biognosys' iRT kit calibration peptides.

### LC-MS/MS acquisition

For phospho-proteome liquid chromatography-tandem mass spectrometry (LC-MS/MS) hyper reaction monitoring (HRM) measurements, 7 μL sample was injected to an in-house packed reversed phase column (PicoFrit emitter with 75 μm inner diameter, 60 cm length, and 10 μm tip from New Objective, packed with 1.7 μm Charged Surface Hybrid C18 particles from Waters) on a Thermo Fisher Scientific EASY nLC 1200 nano liquid chromatography system connected to a Thermo Fisher Scientific Q Exactive HF X mass spectrometer equipped with a Nanospray Flex ion source LC solvents (A) 0.1% formic acid in water and (B) 20% water in acetonitrile with 0.1% formic acid. A DIA method with one full range survey scan and 29 DIA windows was adopted from Bruderer et al.[57]

### Spectral library generation and HRM data analysis

The HRM mass spectrometric data were searched using SpectroMine software (version 3.0) the false discovery rate on peptide and protein level was set to 1. A human UniProt FASTA database was used for the search engine, allowing for 2 missed cleavages and variable modifications (N-terminal acetylation, methionine oxidation, and phosphorylation [STY]). A direct DIA spectral library was created from the search results by filtering for phosphorylated peptides. HRM mass spectrometric data were analyzed using Spectronaut software (version 15.4, Biognosys). The FDR on peptide and protein level was set to 1%, and the data were filtered using row-based extraction. The direct DIA spectral library generated in this project was used for the analysis. The HRM measurements analyzed with Spectronaut were normalized using local regression normalization.[58] Data were filtered to contain only protein hits present in all 3 replicates of at least one treatment group. Missing data were imputed using random draws from a Gaussian distribution centered around a minimal value (0.01 quantile) with a standard deviation estimated as the median protein-wise standard deviation. $p$ values were determined using a two-sample Student's t test and adjusted for a false discovery rate of 0.05 using the Benjamini-Hochberg procedure.

## NF-κB response element luciferase assay

Suspension-adapted HEK293T cells were co-transfected with 3$^{rd}$ generation LV plasmids (as previously described) and 0.06 μg/mL NanoLuc Reporter Vector with 5× NF-κB Response Element (N1111, Promega). Cells were treated with inducing agents or with 20 ng/mL recombinant human TNF-α (hTNF-α) (210-TA, R&D Systems) reconstituted in PBS + 0.1% BSA (A9418, Merck) as

positive control 22 h after transfection. PBS + 0.1% BSA was used as carrier control. At 5 h post-induction, $1 \times 10^5$ cells were mixed with Nano-Glo Luciferase Assay Reagent (N1110, Promega) as per kit instructions. Luminescence was measured using a SpectraMax i3x (Molecular Devices) with an integration time of 10 s per well.

### Statistical analysis

Statistical analysis was performed by Welch's unequal variances t test (two-tailed) in GraphPad Prism (version 9.2). $p < 0.05$ was considered significant.

## DATA AVAILABILITY

The authors declare that the data supporting the findings of this study are included within the article and its supplemental information file, or are available from the authors on request, subject to a confidentiality agreement.

## ACKNOWLEDGMENTS

The work in this manuscript was fully funded by Oxford Biomedica (UK) Ltd.

## AUTHOR CONTRIBUTIONS

C.M-K. and R.A.S.R. designed experiments. C.M-K. conducted experiments and analyzed data. R.R. performed peptide mass spectrometry and data analysis. B.M.A. and J.W. engineered vector and 256U1 plasmid sequences. T.E. and A.K. contributed to study design and analysis. C.M-K. prepared the manuscript with input from all authors. R.A.S.R., K.A.M., D.C.F., and N.G.C. provided resources, supervision, and project administration. All authors have read and approved the manuscript.

## DECLARATION OF INTERESTS

The work described was fully funded by Oxford Biomedica (UK) Ltd., and all authors at the time of submission were employees and hold stock or stock options within the company. The authors declare that a patent application has been submitted related to this work (patent application no. WO/2021/229242), assigned to Oxford Biomedica (UK) Ltd.

## SUPPLEMENTAL INFORMATION

Supplemental information can be found online at https://doi.org/10.1016/j.omtm.2025.101484.

## REFERENCES


1. Naldini, L., Blömer, U., Gallay, P., Ory, D., Mulligan, R., Gage, F.H., Verma, I.M., and Trono, D. (1996). In vivo gene delivery and stable transduction of nondividing cells by a lentiviral vector. Science *272*, 263–267. https://doi.org/10.1126/science.272.5259.263.
2. Wolff, J.H., and Mikkelsen, J.G. (2022). Delivering genes with human immunodeficiency virus-derived vehicles: still state-of-the-art after 25 years. J. Biomed. Sci. *29*, 79. https://doi.org/10.1186/s12929-022-00865-4.
3. Reeves, R., Gorman, C.M., and Howard, B. (1985). Minichromosome assembly of non-integrated plasmid DNA transfected into mammalian cells. Nucleic Acids Res. *13*, 3599–3615. https://doi.org/10.1093/nar/13.10.3599.
4. Jaalouk, D.E., Crosato, M., Brodt, P., and Galipeau, J. (2006). Inhibition of histone deacetylation in 293GPG packaging cell line improves the production of self-inactivating MLV-derived retroviral vectors. Virol. J. *3*, 27. https://doi.org/10.1186/1743-422X-3-27.
5. de Vries, W., Haasnoot, J., van der Velden, J., van Montfort, T., Zorgdrager, F., Paxton, W., Cornelissen, M., van Kuppeveld, F., de Haan, P., and Berkhout, B. (2008). Increased virus replication in mammalian cells by blocking intracellular innate defense responses. Gene Ther. *15*, 545–552. https://doi.org/10.1038/gt.2008.12.
6. Colomer-Lluch, M., Ruiz, A., Moris, A., and Prado, J.G. (2018). Restriction Factors: From Intrinsic Viral Restriction to Shaping Cellular Immunity Against HIV-1. Front. Immunol. *9*, 2876. https://doi.org/10.3389/fimmu.2018.02876.
7. Han, J., Tam, K., Ma, F., Tam, C., Aleshe, B., Wang, X., Quintos, J.P., Morselli, M., Pellegrini, M., Hollis, R.P., and Kohn, D.B. (2021). β-Globin Lentiviral Vectors Have Reduced Titers due to Incomplete Vector RNA Genomes and Lowered Virion Production. Stem Cell Rep. *16*, 198–211. https://doi.org/10.1016/j.stemcr.2020.10.007.
8. Ferreira, C.B., Sumner, R.P., Rodriguez-Plata, M.T., Rasaiyaah, J., Milne, R.S., Thrasher, A.J., Qasim, W., and Towers, G.J. (2020). Lentiviral Vector Production Titer Is Not Limited in HEK293T by Induced Intracellular Innate Immunity. Mol. Ther. Methods Clin. Dev. *17*, 209–219. https://doi.org/10.1016/j.omtm.2019.11.021.
9. Maunder, H.E., Wright, J., Kolli, B.R., Vieira, C.R., Mkandawire, T.T., Tatoris, S., Kennedy, V., Iqball, S., Devarajan, G., Ellis, S., et al. (2017). Enhancing titres of therapeutic viral vectors using the transgene repression in vector production (TRiP) system. Nat. Commun. *8*, 14834. https://doi.org/10.1038/ncomms14834.
10. Poletti, V., and Mavilio, F. (2021). Designing Lentiviral Vectors for Gene Therapy of Genetic Diseases. Viruses *13*, 1526. https://doi.org/10.3390/v13081526.
11. Ansorge, S., Lanthier, S., Transfiguracion, J., Durocher, Y., Henry, O., and Kamen, A. (2009). Development of a scalable process for high-yield lentiviral vector production by transient transfection of HEK293 suspension cultures. J. Gene Med. *11*, 868–876. https://doi.org/10.1002/jgm.1370.
12. Broussau, S., Lytvyn, V., Simoneau, M., Guilbault, C., Leclerc, M., Nazemi-Moghaddam, N., Coulombe, N., Elahi, S.M., McComb, S., and Gilbert, R. (2023). Packaging cells for lentiviral vectors generated using the cumate and coumermycin gene induction systems and nanowell single-cell cloning. Mol. Ther. Methods Clin. Dev. *29*, 40–57. https://doi.org/10.1016/j.omtm.2023.02.013.
13. Cribbs, A.P., Kennedy, A., Gregory, B., and Brennan, F.M. (2013). Simplified production and concentration of lentiviral vectors to achieve high transduction in primary human T cells. BMC Biotechnol. *13*, 98. https://doi.org/10.1186/1472-6750-13-98.
14. Tridgett, M., Mulet, M., Johny, S.P., Ababi, M., Raghunath, M., Fustinoni, C., Galabova, B., Fernández-Díaz, C., Mikalajūnaitė, I., Tomás, H.A., et al. (2024). Lentiviral vector packaging and producer cell lines yield titers equivalent to the industry-standard four-plasmid process. Mol. Ther. Methods Clin. Dev. *32*, 101315. https://doi.org/10.1016/j.omtm.2024.101315.
15. Seto, E., and Yoshida, M. (2014). Erasers of Histone Acetylation: The Histone Deacetylase Enzymes. Cold Spring Harbor Perspect. Biol. *6*, a018713. https://doi.org/10.1101/cshperspect.a018713.
16. Gallinari, P., Di Marco, S., Jones, P., Pallaoro, M., and Steinkühler, C. (2007). HDACs, histone deacetylation and gene transcription: from molecular biology to cancer therapeutics. Cell Res. *17*, 195–211. https://doi.org/10.1038/sj.cr.7310149.
17. Fillot, T., and Mazza, D. (2025). Rethinking chromatin accessibility: from compaction to dynamic interactions. Curr. Opin. Genet. Dev. *90*, 102299. https://doi.org/10.1016/j.gde.2024.102299.
18. Suzuki, N., Yoshida, T., Takeuchi, H., Sakuma, R., Sukegawa, S., and Yamaoka, S. (2018). Robust Enhancement of Lentivirus Production by Promoter Activation. Sci. Rep. *8*, 15036. https://doi.org/10.1038/s41598-018-33042-5.
19. Han, J., Tam, K., Tam, C., Hollis, R.P., and Kohn, D.B. (2021). Improved lentiviral vector titers from a multi-gene knockout packaging line. Mol. Ther. Oncolytics *23*, 582–592. https://doi.org/10.1016/j.omto.2021.11.012.
20. Farley, D., and Wright, J. (2021). Enhancing production of lentiviral vectors. Patent Application #WO/2021/014157 (Oxford Biomedica (UK) Limited).
21. Wright, J., Alberts, B.M., Hood, A.J., Nogueira, C., Miskolczi, Z., Vieira, C.R., Chipchase, D., Lamont, C.M., Goodyear, O., Moyce, L.J., et al. (2024). Improved Production and Quality of Lentiviral Vectors By Major-Splice-Donor Mutation and Co-Expression of a Novel U1 Snrna-Based Enhancer. Preprint at Social Science Research Network. https://doi.org/10.2139/ssrn.4929949.
22. Lenz, J.C., Reusch, H.P., Albrecht, N., Schultz, G., and Schaefer, M. (2002). Ca2+-controlled competitive diacylglycerol binding of protein kinase C isoenzymes in living cells. J. Cell Biol. *159*, 291–302. https://doi.org/10.1083/jcb.200203048.
23. Kazanietz, M.G., and Cooke, M. (2024). Protein kinase C signaling "in" and "to" the nucleus: Master kinases in transcriptional regulation. J. Biol. Chem. *300*, 105692. https://doi.org/10.1016/j.jbc.2024.105692.
24. Kulkosky, J., Culnan, D.M., Roman, J., Dornadula, G., Schnell, M., Boyd, M.R., and Pomerantz, R.J. (2001). Prostratin: activation of latent HIV-1 expression suggests a

potential inductive adjuvant therapy for HAART. Blood *98*, 3006–3015. https://doi.org/10.1182/blood.v98.10.3006.

25. Brogdon, J., Ziani, W., Wang, X., Veazey, R.S., and Xu, H. (2016). In vitro effects of the small-molecule protein kinase C agonists on HIV latency reactivation. Sci. Rep. *6*, 39032. https://doi.org/10.1038/srep39032.
26. Williams, S.A., Chen, L.-F., Kwon, H., Fenard, D., Bisgrove, D., Verdin, E., and Greene, W.C. (2004). Prostratin antagonizes HIV latency by activating NF-kappaB. J. Biol. Chem. *279*, 42008–42017. https://doi.org/10.1074/jbc.M402124200.
27. Jiang, G., Mendes, E.A., Kaiser, P., Wong, D.P., Tang, Y., Cai, I., Fenton, A., Melcher, G.P., Hildreth, J.E.K., Thompson, G.R., et al. (2015). Synergistic Reactivation of Latent HIV Expression by Ingenol-3-Angelate, PEP005, Targeted NF-kB Signaling in Combination with JQ1 Induced p-TEFb Activation. PLoS Pathog. *11*, e1005066. https://doi.org/10.1371/journal.ppat.1005066.
28. Pluta, A., Jaworski, J.P., and Cortés-Rubio, C.N. (2020). Balance between Retroviral Latency and Transcription: Based on HIV Model. Pathogens *10*, 16. https://doi.org/10.3390/pathogens10010016.
29. Ne, E., Palstra, R.-J., and Mahmoudi, T. (2018). Transcription: Insights From the HIV-1 Promoter. Int. Rev. Cell Mol. Biol. *335*, 191–243. https://doi.org/10.1016/bs.ircmb.2017.07.011.
30. Harrop, R., Blount, D.G., Khan, N., Soyombo, M., Moyce, L., Drayson, M.T., Down, J., Lawson, M.A., O'Connor, D., Nimmo, R., et al. (2025). Targeting Tumor Antigen 5T4 Using CAR T Cells for the Treatment of Acute Myeloid Leukemia. Mol. Cancer Therapeut. *24*, 93–104. https://doi.org/10.1158/1535-7163.MCT-24-0052.
31. Ali, F.R., Wlodek, C., and Lear, J.T. (2012). The role of ingenol mebutate in the treatment of actinic keratoses. Dermatol. Ther. *2*, 8. https://doi.org/10.1007/s13555-012-0008-4.
32. Bahrami, S., and Drabløs, F. (2016). Gene regulation in the immediate-early response process. Adv. Biol. Regul. *62*, 37–49. https://doi.org/10.1016/j.jbior.2016.05.001.
33. Szklarczyk, D., Kirsch, R., Koutrouli, M., Nastou, K., Mehryary, F., Hachilif, R., Gable, A.L., Fang, T., Doncheva, N.T., Pyysalo, S., et al. (2023). The STRING database in 2023: protein-protein association networks and functional enrichment analyses for any sequenced genome of interest. Nucleic Acids Res. *51*, D638–D646. https://doi.org/10.1093/nar/gkac1000.
34. Kumbrink, J., Gerlinger, M., and Johnson, J.P. (2005). Egr-1 Induces the Expression of Its Corepressor Nab2 by Activation of the Nab2 Promoter Thereby Establishing a Negative Feedback Loop. J. Biol. Chem. *280*, 42785–42793. https://doi.org/10.1074/jbc.M511079200.
35. Balko, J.M., Schwarz, L.J., Bhola, N.E., Kurupi, R., Owens, P., Miller, T.W., Gómez, H., Cook, R.S., and Arteaga, C.L. (2013). Activation of MAPK pathways due to DUSP4 loss promotes cancer stem cell-like phenotypes in basal-like breast cancer. Cancer Res. *73*, 6346–6358. https://doi.org/10.1158/0008-5472.CAN-13-1385.
36. Chen, E.Y., Tan, C.M., Kou, Y., Duan, Q., Wang, Z., Meirelles, G.V., Clark, N.R., and Ma'ayan, A. (2013). Enrichr: interactive and collaborative HTML5 gene list enrichment analysis tool. BMC Bioinf. *14*, 128. https://doi.org/10.1186/1471-2105-14-128.
37. Wiredja, D.D., Koyutürk, M., and Chance, M.R. (2017). The KSEA App: a web-based tool for kinase activity inference from quantitative phosphoproteomics. Bioinformatics *33*, 3489–3491. https://doi.org/10.1093/bioinformatics/btx415.
38. Zhou, Y., Zhou, B., Pache, L., Chang, M., Khodabakhshi, A.H., Tanaseichuk, O., Benner, C., and Chanda, S.K. (2019). Metascape provides a biologist-oriented resource for the analysis of systems-level datasets. Nat. Commun. *10*, 1523. https://doi.org/10.1038/s41467-019-09234-6.
39. Merten, O.-W., Charrier, S., Laroudie, N., Fauchille, S., Dugué, C., Jenny, C., Audit, M., Zanta-Boussif, M.-A., Chautard, H., Radrizzani, M., et al. (2011). Large-scale manufacture and characterization of a lentiviral vector produced for clinical ex vivo gene therapy application. Hum. Gene Ther. *22*, 343–356. https://doi.org/10.1089/hum.2010.060.
40. Merten, O.-W., Hebben, M., and Bovolenta, C. (2016). Production of lentiviral vectors. Mol. Ther. Methods Clin. Dev. *3*, 16017. https://doi.org/10.1038/mtm.2016.17.
41. Tan, E., Chin, C.S.H., Lim, Z.F.S., and Ng, S.K. (2021). HEK293 Cell Line as a Platform to Produce Recombinant Proteins and Viral Vectors. Front. Bioeng. Biotechnol. *9*, 796991. https://doi.org/10.3389/fbioe.2021.796991.
42. Olsen, J.C., and Sechelski, J. (1995). Use of sodium butyrate to enhance production of retroviral vectors expressing CFTR cDNA. Hum. Gene Ther. *6*, 1195–1202. https://doi.org/10.1089/hum.1995.6.9-1195.
43. Wang, B., Guo, H., Yu, H., Chen, Y., Xu, H., and Zhao, G. (2021). The Role of the Transcription Factor EGR1 in Cancer. Front. Oncol. *11*, 642547. https://doi.org/10.3389/fonc.2021.642547.
44. Angel, P., Imagawa, M., Chiu, R., Stein, B., Imbra, R.J., Rahmsdorf, H.J., Jonat, C., Herrlich, P., and Karin, M. (1987). Phorbol ester-inducible genes contain a common cis element recognized by a TPA-modulated trans-acting factor. Cell *49*, 729–739. https://doi.org/10.1016/0092-8674(87)90611-8.
45. Krishna, B.A., Wass, A.B., and O'Connor, C.M. (2020). Activator protein-1 transactivation of the major immediate early locus is a determinant of cytomegalovirus reactivation from latency. Proc. Natl. Acad. Sci. USA *117*, 20860–20867. https://doi.org/10.1073/pnas.2009420117.
46. Johari, Y.B., Scarrott, J.M., Pohle, T.H., Liu, P., Mayer, A., Brown, A.J., and James, D.C. (2022). Engineering of the CMV promoter for controlled expression of recombinant genes in HEK293 cells. Biotechnol. J. *17*, e2200062. https://doi.org/10.1002/biot.202200062.
47. Schoggins, J.W., Wilson, S.J., Panis, M., Murphy, M.Y., Jones, C.T., Bieniasz, P., and Rice, C.M. (2011). A diverse range of gene products are effectors of the type I interferon antiviral response. Nature *472*, 481–485. https://doi.org/10.1038/nature09907.
48. Leonard, B., McCann, J.L., Starrett, G.J., Kosyakovsky, L., Luengas, E.M., Molan, A.M., Burns, M.B., McDougle, R.M., Parker, P.J., Brown, W.L., and Harris, R.S. (2015). The PKC/NF-κB signaling pathway induces APOBEC3B expression in multiple human cancers. Cancer Res. *75*, 4538–4547. https://doi.org/10.1158/0008-5472.CAN-15-2171-T.
49. Lim, P.S., Sutton, C.R., and Rao, S. (2015). Protein kinase C in the immune system: from signalling to chromatin regulation. Immunology *146*, 508–522. https://doi.org/10.1111/imm.12510.
50. Santoro, M.G., Rossi, A., and Amici, C. (2003). NF-κB and virus infection: who controls whom. EMBO J. *22*, 2552–2560. https://doi.org/10.1093/emboj/cdg267.
51. Jeronimo, C., Collin, P., and Robert, F. (2016). The RNA Polymerase II CTD: The Increasing Complexity of a Low-Complexity Protein Domain. J. Mol. Biol. *428*, 2607–2622. https://doi.org/10.1016/j.jmb.2016.02.006.
52. Pundhir, S., Su, J., Tapia, M., Hansen, A.M., Haile, J.S., Hansen, K., and Porse, B.T. (2023). The impact of SWI/SNF and NuRD inactivation on gene expression is tightly coupled with levels of RNA polymerase II occupancy at promoters. Genome Res. *33*, 332–345. https://doi.org/10.1101/gr.277089.122.
53. Li, J., Duns, G., Westers, H., Sijmons, R., van den Berg, A., and Kok, K. (2016). SETD2: an epigenetic modifier with tumor suppressor functionality. Oncotarget *7*, 50719–50734. https://doi.org/10.18632/oncotarget.9368.
54. Kim, V.N., Mitrophanous, K., Kingsman, S.M., and Kingsman, A.J. (1998). Minimal requirement for a lentivirus vector based on human immunodeficiency virus type 1. J. Virol. *72*, 811–816. https://doi.org/10.1128/JVI.72.1.811-816.1998.
55. Kotsopoulou, E., Kim, V.N., Kingsman, A.J., Kingsman, S.M., and Mitrophanous, K.A. (2000). A Rev-independent human immunodeficiency virus type 1 (HIV-1)-based vector that exploits a codon-optimized HIV-1 gag-pol gene. J. Virol. *74*, 4839–4852. https://doi.org/10.1128/jvi.74.10.4839-4852.2000.
56. Farley, D.C., Iqball, S., Smith, J.C., Miskin, J.E., Kingsman, S.M., and Mitrophanous, K.A. (2007). Factors that influence VSV-G pseudotyping and transduction efficiency of lentiviral vectors-in vitro and in vivo implications. J. Gene Med. *9*, 345–356. https://doi.org/10.1002/jgm.1022.
57. Bruderer, R., Bernhardt, O.M., Gandhi, T., Miladinović, S.M., Cheng, L.-Y., Messner, S., Ehrenberger, T., Zanotelli, V., Butscheid, Y., Escher, C., et al. (2015). Extending the limits of quantitative proteome profiling with data-independent acquisition and application to acetaminophen-treated three-dimensional liver microtissues. Mol. Cell. Proteomics *14*, 1400–1410. https://doi.org/10.1074/mcp.M114.044305.
58. Callister, S.J., Barry, R.C., Adkins, J.N., Johnson, E.T., Qian, W.-J., Webb-Robertson, B.-J.M., Smith, R.D., and Lipton, M.S. (2006). Normalization approaches for removing systematic biases associated with mass spectrometry and label-free proteomics. J. Proteome Res. *5*, 277–286. https://doi.org/10.1021/pr050300l.